Title

Excess Lithium in Transition Metal Layers of Epitaxially Grown Thin Film Cathodes of Li2MnO3 Leads to Rapid Loss of Covalency during First Battery Cycle

Journal

The Journal of Physical Chemistry C, 123(47)

ISSN

1932-7447

Authors

Massel, Felix
Hikima, Kazuhiro
Rensmo, Håkan
et al.

Publication Date

2019-11-27

DOI

10.1021/acs.jpcc.9b06246

Excess lithium in transition metal layers leads to rapid loss of covalency during cycling of epitaxially grown Li_2MnO_3-cathodes

Felix Massel[1], Kazuhiro Hikima[2,3], Maria Hahlin[1], Håkan Rensmo[1], Kota Suzuki[2], Masaaki Hirayama[2], Chao Xu[4], Reza Younesi[4], Yi-Sheng Liu[5], Jinghua Guo[5], Ryoji. Kanno[2] and Laurent-Clausius Duda[1]

***Abstract*— We have investigated the initial-cycle battery behavior of epitaxial thin films of Li_2MnO_3-cathodes by employing resonant inelastic X-ray scattering (RIXS) at the O K- and Mn L_3-edges. Thin films (25 nm thickness) with Li/Mn-ratios of 2.06 (*stoichiometric*) and 2.27 (*over-stoichiometric*), respectively, were epitaxially grown by pulsed laser deposition and electrochemically cycled as battery cathodes in half-cell setup, stopped at potentials for full charge (delithiation) and complete discharge (relithiation), respectively, for X-ray analysis. Using RIXS, we find that significant anionic reactions take place in both materials upon initial delithiation. However, no signatures of localized oxygen holes are found in O K-RIXS of the Li_2MnO_3 regardless of Li/Mn-ratio. Instead, the top of the oxygen valence band is depleted of electrons forming delocalized empty states. Concomitantly, Mn L-RIXS of the over-stoichiometric cathode material shows a rapid loss of Mn–O hybridization whereas the hybridization is significantly more stable in the stoichiometric material.**

I. Introduction

In the quest for higher-capacity rechargable batteries, Li-rich, layered, high-voltage Mn-oxide based cathode materials are currently receiving much attention due to their *extra* capacity, i. e. capacity beyond the limit expected from their cationic redox reactions alone [1]. One has found strong evidence [2] that much of the extra capacity in such materials in which Mn is partially substituted by Ni and Co, so-called Li-rich NMC-materials, derives from reversible anionic processes that take place already in the initial cycle. In contrast, it is well-known that the first charge of the Ni- and Co-free end member $Li[Li_{1/3}Mn_{2/3}]O_2$ (or Li_2MnO_3) has an *activation phase* in which structural transformations take place. In this activation phase, charge compensation in connection with migration of metal ions and loss of oxygen from the material contributes to the recorded charge capacity. The origin for this difference in behavior of Li-rich NMC and Li_2MnO_3 has still not been explained satisfyingly so far. Thus it is desirable to understand and to be able to control the conditions under which anionic processes lends reversible extra capacity to this kind of materials.

A density functional theory based simulation study of Li_2MnO_3 has shown [3] that delithiation leads to an initial oxidation of lattice oxygen while manganese ions are expected to remain in a Mn^{4+}-state. This would seem to be favorable for expecting the same kind of reversible anionic redox reactions to occur as in the Li-rich NMC-materials. However, the oxygen hole states are not stable and decay before a reversible discharge can commence. Instead there is a lattice restructuring, including Mn-migration to the Li-layers, and the formation of oxygen gas. However, experimentally it was instead found [4] that there is an appreciable formation of Mn^{3+}- (and to a lesser degree of Mn^{2+}-) ions upon delithiation. Relithiation lets the Mn^{3+}-ion content rise to a level above 80%. In the reversible cycling phase it is the $Mn^{3+/4+}$-redox couple that is assumed to charge compensate for (de-)lithiation. Thus it is necessary to gather additional information to gain a better understanding about the details of the redox processes of Li_2MnO_3.

Epitaxial thin films of Li_2MnO_3 composition can be grown with high quality [5] and are suitable for use as a cathode material in connection with liquid electrolyte cells or as part of all-solid-state batteries [6]. Thin film cathodes work without conductive carbon and a binder, both of which are common ingredients in commercial lithium batteries that have an active material in form of polycrystalline, micron sized particles. It is evident that studies of cathode materials grown as epitaxial thin film offer a number of advantages. The complexity inherent to a polycrystalline composite materials is reduced and, for instance, the role of a homogeneous interface can be studied in detail given the 2D geometry.

Fig. 1 shows a schematic of a typical epitaxially grown film and the crystal structure [5] of the active cathode material, Li_2MnO_3. The surface (top) of the active cathode material is atomically flat and, when incorporated in a battery, forms an immediate interface with the electrolyte (not depicted) over the entire area. Such Li_2MnO_3 films can be synthesized with controlled variation of the film stoichiometry. By tuning the film's Li/Mn-ratio, we have the possibility to learn more about the redox processes that govern Li_2MnO_3 materials. For instance, the initial Li/Mn-ratio [7] and the film thickness [5] has a direct influence on the initial delithiation (charging) capacity. More interestingly, studies have also shown that the Li/Mn-ratio is a crucial factor for both the capacity retention in the first relithiation (discharge) as well as the fading properties of the cathode in

[1]*Department of Physics and Astronomy, Division of Molecular and Condensed Matter Physics, Uppsala University, Box 516, S-751 20 Uppsala, Sweden*

[2]*Department of Chemical Science and Engineering, School of Materials and chemical Technology, Tokyo Institute of Technology, 4259 Nagatsuta-cho, Midori-ku, Yokohama 226-8502, Japan*

[3]*Department of Electrical and Electronic Information Engineering, Toyohashi University of Technology, 1-1 Hibarigaoka, Tempaku, Toyohashi, Aichi 441-8580, Japan*

[4]*Department of Chemistry - Ångström Laboratory, Structural Chemistry, Uppsala University, Box 538, 751 21 Uppsala, Sweden*

[5]*Advanced Light Source, Lawrence Berkeley Laboratory, Berkeley, CA, USA*

repeated cycling [7]. Furthermore, very thin films (12.6 nm) have been found to exhibit slightly increasing capacity (after the first relithiation) up to at least the 50$^{\text{th}}$ cycle. These initial results promise interesting opportunities for obtaining a better understanding of the role of the activation process of Li_2MnO_3, particularly because the composition, thickness, and crystal orientation can be controlled. Previously [5], epitaxial LMO-films with under-stoichiometric Li-content was studied, some of which show capacities exceeding that of common polycrystalline Li_2MnO_3.

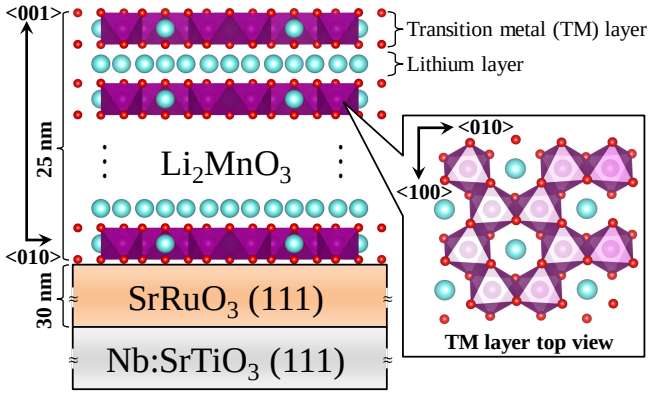

Fig. 1. Schematic of the grown multilayer film with details of the Li_2MnO_3 crystal structure: light blue spheres represent Li^+ ions and purple octahedra with red spheres on the corners depict MnO_6. The latter have a honeycomb arrangement effectively offering 1D pathways for lithium diffusion as seen in the top view. Adapted from [6].

In this work we have studied epitaxial thin films of Li_2MnO_3 at two different Li/Mn-ratios $r_{\text{Li/Mn}} = 2.07$ (denoted *stoichiometric*) and $r_{\text{Li/Mn}} = 2.26$ (denoted *over-stoichiometric*). The first film ($r_{\text{Li/Mn}} = 2.07$) is close to having stoichiometric Li content where $1/3$ of the Li-ions reside in the metal-oxide layer. The other film ($r_{\text{Li/Mn}} = 2.26$) has a higher, Li-rich content. Our goal in the present study is to investigate the nature of the activation phase that takes place in the first de- and relithiation (charge and discharge) cycle as a function of the Li/Mn-ratio and to investigate the nature of the redox processes. For this we employed RIXS and XAS at the Mn L- and O K-absorption edges that lend insight into the changes of the electronic structure in the films. We find that the activation process of both materials is governed by significant irreversible changes of the electronic structure. This includes changes of the manganese oxidation state as well as a variation of oxygen hole states. Mn L- and O K-RIXS reveal a strong dependence of the Mn–O bond covalency on the initial Li/Mn-ratio in the first cycle.

II. Experimental

A. Epitaxial Growth of Cathode Films

Li_2MnO_3/$SrRuO_3$ multi-layer epitaxial thin films with a thickness of 25 nm were grown using pulsed laser deposition (PLD). The substrates used were single crystals of Nb-doped $SrTiO_3$ (0.5% Nb, $(10 \times 10 \times 5)\,\text{mm}^3$ in size) with a (1 1 1) orientation. Pretreatment of the substrates included washing with ultra pure water and annealing at 1000°C. The PLD process was performed using a KrF excimer laser (Lambda Physik, COMPex102 and 201) with a wavelength of 248 nm and a vacuum chamber (AOV Inc., PSAD-3000). Prior to cathode film deposition, a 30 nm layer of $SrRuO_3$ was grown as a current collector [8]. The thin film compositions were controlled by target composition and oxygen pressure. $Li_{2.1}MnO_3$ (5% lithium excess) and $Li_{2.4}MnO_3$ (20% lithium excess) sintered pellets (Toshima Manufacturing Co., Ltd.) were used. During PLD the substrate-target distance was 60 mm, substrate temperature was 923 K, laser frequency was 3 Hz, deposition time was 10 min, laser energy was 1.1 J cm^{-2}, and O_2 partial pressure was 75 Pa.

A total number of six epitaxial cathode films were synthesized with two different Li contents: a set of stoichiometric composition, $Li_{2.00}Mn_{0.97}O_{2.94}$, and a set with over-stoichiometric composition, $Li_{2.06}Mn_{0.91}O_{2.84}$. The Li/Mn-ratios of the pristine films are $r_{\text{Li/Mn}} = 2.07$ and 2.26, respectively. Fig. 1 shows a schematic of the structure of the multilayer films as well as the crystal structure [5] of a stoichiometric Li_2MnO_3 material.

B. Electrochemical Cycling

For each set two films were assembled to a working battery in a pouch cell containing a 1:1 mixture of EC:DEC as electrolyte (BASF Co., Ltd.) and Li metal as anode. Electrochemical cycling was performed using a Arbin Instruments potentiostat. All films were cycled under a constant current mode with 1.5 µA at a C-rate of 1.5 C. In order to ensure near complete de- and relithiation of the films, the cycling was terminated after reaching the two different cell potentials of 4.8 and 2.0 V vs. Li/Li^+ labeled as *end of charge* (*EoC*) and *end of discharge* (*EoD*), respectively. Films marked *pristine* were not cycled or exposed to the electrolyte. The charge-discharge curves of the films are shown in Fig. S1 of the supplementary information (SI). The charge-discharge behavior for both films is very similar to that reported for polycrystalline Li_2MnO_3 [4], with a long voltage plateau at 4.6 V and and a first-cycle discharge capacity that is approximately 50% and 60% smaller (over-stoichiometric and stoichiometric films, respectively) than the initial charge capacity.

While the initial cycling behaviors of both compositions show only small differences, long term cycling experiments [7] reveal considerably stronger capacity fading of over-stoichiometric films compared to the stoichiometric films. The latter even exhibit some recovering from the initial capacity loss.

C. X-ray Spectroscopy

The cycled batteries were disassembled in a glove box, the cathode films were rinsed and sealed under Ar and then transported to Beamline 8.0.1 [9] at the Advanced Light Source (ALS), Lawrence Berkeley Laboratory, USA. The beamline is equipped with a spherical grating monochromator and a photon flux of about 10^{11} photons/sec/0.01%

bandwidth can be focused to a spot size smaller than $(35 \times 100)\,\mu m^2$ (vertically $\times$ horizontally). The storage ring operates in a quasi-constant top-off mode, delivering stable photon fluxes averaged over several minutes. X-ray absorption spectroscopy (XAS) as well as resonant inelastic X-ray scattering (RIXS) at the O K- and Mn L-edge were performed.

The bulk-sensitive total fluorescence yield (TFY) mode of XAS ($\sim$100 nm probing depth) was obtained using a channeltron in a negative potential setting to reject the photoelectrons. The more surface sensitive TEY mode of XAS ($\sim$10 nm probing depth) was recorded simultaneously by measuring the sample drain current at each incident energy. A monochromator band pass of 0.1 to 0.2 eV was used, depending on incident energy. Energy calibration of the XAS spectra was achieved by recording O K-edge spectra of a TiO_2 standard. All XAS spectra were normalized by division of an I_0-signal obtained from a Au-coated grid placed downstream of the last refocusing mirror. A background was subtracted from each spectrum by fitting to the pre-threshold energy region and subsequently the atomic step was normalized to unity.

O K-pre- and Mn L_3-edge RIXS spectra were recorded using a high-resolution VLS-grating spectrometer [9]. The monochromator and spectrometer resolution were 0.5 eV, respectively. A monochromator-reading energy offset of 6.4 eV was determined by measuring the O K-edge of a TiO_2 reference sample and have been corrected for in all spectra presented. XAS spectra were normalized to incident flux and when necessary background was subtracted before scaling to unit atomic step. Note that we have employed a grazing incidence ($\leq 20°$) geometry ensuring, particularly when recording O K-edge XAS and RIXS spectra, minimal contribution from the underlying layers of Nb:$SrTiO_3$ and $SrRuO_3$. In Fig. S3 of the SI we present difference spectra that verify minimal contribution from the substrate layers.

III. Results

A. O K- and Mn L-XAS

Fig. 2 shows TEY-signal O K-edge XAS at three states of charge of the initial battery cycle of films with stoichiometric and over-stoichiometric composition, upper and lower spectra respectively: (i) pristine (black traces), (ii) fully delithiated (EoC, red traces) and (iii) relithiated (EoD, green traces). The more bulk-sensitive TFY-signal spectra are shown in Fig. S2 of the SI and are largely consistent with the more surface-sensitive spectra of Fig. 2, pointing to a homogeneous electronic structure of oxygen throughout the films.

The pre-peak range, 528 to 534 eV, reflects the local density of empty electronic states on oxygen $2p$-orbitals that hybridize strongly with Mn $3d$-orbitals [10], [11]. The pre-edge region for both compositions features two distinct peaks at 529.7 eV and 531.9 eV. The O K-edge XAS of the pristine materials (black traces) resemble the spectra of MnO_2 [12], which is consistent with the stoichiometry of Li_2MnO_3.

After first delithiation (EoC, red traces) especially the O K-XAS pre-peaks show a broadening and an intensity increase. This goes for both compositions (consistent with ref. [4]), whereby the broadening and intensity increase is more pronounced in the over-stoichiometric film.

Subsequent first relithiation (EoD, green traces) leads to an intensity decrease of the O K-XAS pre-peaks as well as a substantial increase of the main edge structures above 534 eV. Note however the large difference between the films in this state: The over-stoichiometric film material shows a more dramatic intensity decrease than the stoichiometric film and a significant peak emerges at 533.8 eV (in TEY as well as in TFY, though somewhat weaker). This peak has been observed before in the composite material [4], however, its origin is unclear. Somewhat surprisingly, the results from the over-stoichiometric film are more similar to ref. [4].

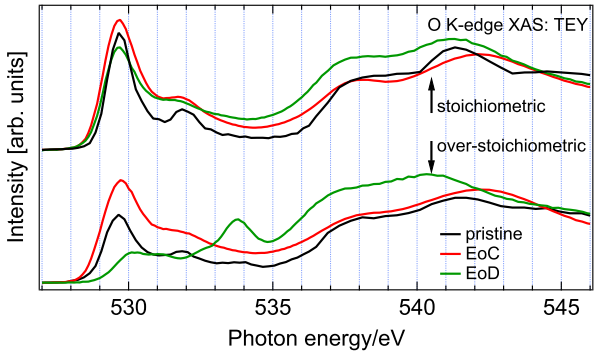

Fig. 2. TEY-signal O K-edge XAS of films with stoichiometric and over-stoichiometric composition, upper and lower spectra respectively, at the first cycle states of charge: pristine (black), delithiated (red, EoC), and relithiated (green, EoD).

Fig. 3 shows the corresponding Mn L-XAS spectra of the TEY-signal. We also include reference spectra of polycrystalline manganese oxide materials with octahedral site symmetry and formal oxidation states of Mn^{2+}, Mn^{3+}, and Mn^{4+} as they were previously reported by Qiao et al. [13]. The Mn L-edges of both pristine materials clearly exhibit the spectral shape characteristic for Mn^{4+}-ion materials [14], [15], with a distinctive double L_3-peak with main intensity at 643 eV and a single L_2-peak at 653.5 eV (black traces). This is as expected from the stoichiometry of the pristine materials thus the measurement confirms Mn to be in its 4+ valence state before delithiation.

After delithiation the spectral shape of Mn^{4+} is still evident but with additional intensity in the low energy parts (EoC, red traces). We observe an increase of intensity at energies characteristic for Mn^{3+} as well as Mn^{2+} [14], [15]. This suggests that the films after delithiation consist of multiple phases, in which a part of the Mn-ions have been reduced. While this is observed for both compositions, the over-stoichiometric film exhibits stronger manganese reduction.

Upon relithiation we observe a dramatic change of the Mn L-edge (EoD, green traces). The Mn^{4+}-peak at 643 eV is severely reduced for both compositions and instead replaced by Mn^{2+}- and Mn^{3+}-signatures. Mn^{2+} has a sharp leading-edge peak at about 639.7 eV and Mn^{3+} has a broad peak

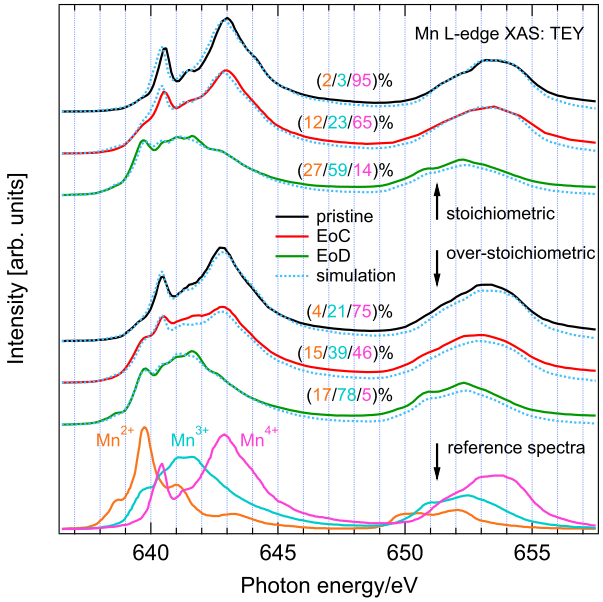

Fig. 3. TEY-signal Mn L-edge XAS of films with stoichiometric and over-stoichiometric composition, upper and middle spectra respectively, at the first cycle states of charge: pristine (black), delithiated (red, EoC), and relithiated (green, EoD). Included at the bottom are reference spectra of manganese oxides with various formal oxidation states: Mn^{2+} (MnO), Mn^{3+} (Mn_2O_3), and Mn^{4+} (Li_2MnO_3); reference spectra as reported by Qiao et al. [13]. Light blue dashed traces represent best-fit linear combinations of the reference spectra with assumed percentiles are given in brackets above each respective simulation.

around 641.5 eV [12], [13], [16]. The Mn^{2+}/Mn^{3+}-ratio is larger for the stoichiometric sample than for the over-stoichiometric sample.

B. O K-RIXS

Fig. 4 shows waterfall plots of energy dependent O K-RIXS spectra for (a) the stoichiometric and (b) over-stoichiometric Li_2MnO_3 films. Here we display excitation energies from threshold (528.5 eV) to the first XAS peak (530.5 eV). The charge-cycle evolution of the Li_2MnO_3 cathodes is visualized by superposed spectra taken at equal incident energies (featuring the same color coding as for the XAS spectra above). Note that the spectra in this plot were normalized to equal maximum intensity to facilitate optimal spectral shape comparison discussed in the following paragraphs. NB: Variations of their integrated intensity normalized to equal incoming flux are reflected in the PFY spectra shown above as insets of Fig. 2.

First, we describe the general features that are characteristic to both film stoichiometries and then we go on to focus on the salient differences between them. The main band of the O K-RIXS spectra (∼520 to 528 eV) is nearly stationary (cf. vertical dashed line at 525.7 eV) in photon energy and therefore assigned to reflect band-like states, i. e. the valence band of O 2p-character (modified to some degree by transition matrix elements). The pristine materials (black traces) display a pronounced high-energy "shoulder", i. e. spectral intensity above the main band, extending all the way to the elastic peak (black arrows, corresponding to the respective incident photon energy). Strikingly, much of that spectral intensity is absent after first delithiation (EoC, red traces) and it does not re-appear upon subsequent relithiation (EoD, green traces). Instead, there is a (quasi-)gap that separates a feature marked by blue arrows and the elastic peak. This suggests that cycling of the pristine material leads to a loss of occupied states close to the Fermi level that are never recovered. The blue arrows are assigned to an excitation process (O 2p–Mn 3d) that leads to excitonic final states, namely Mn dd-excitations mediated by ligand to metal charge transfer [17]. These excitonic excitations reflect the narrow Mn 3d-states and track the elastic peak at a constant energy loss (2.4 eV). This signature is more pronounced in the relithiated over-stoichiometric film, which has a larger fraction of Mn^{3+} ions than the stoichiometric film, suggesting that this belongs to an excitation of an Mn $3d^4$-configuration.

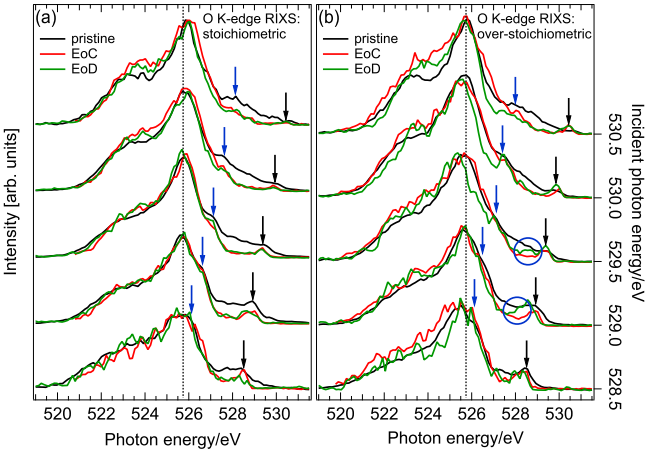

Fig. 4. O K-edge RIXS from the films with (a) stoichiometric and (b) over-stoichiometric composition at different incident photon energies in 0.5 eV steps up to the first absorption pre-edge peak. Blue (black) arrows serve as guides to the eye for the excitonic contributions (elastic peaks). The vertical dashed line serves as reference energy between the two panels. Spectra are normalized to the respective maximum intensity. The complete set of spectra (up to 533.5 eV incident photon energy) is presented in Fig. S4 of the SI.

We now turn to the differences observed in the O K-RIXS of the two film stoichiometries. Whereas the over-stoichiometric films show various spectral differences between the de- and relithiated states this is practically absent in the stoichiometric film. This corroborates the trend found in the O K-XAS and additionally we learn how the occupied O 2p-states behave. In particular, we observe a narrowing of all features in the RIXS spectra only in the case of the over-stoichiometric film upon relithiation to EoD. This leads to a more pronounced excitonic peak at 2.4 eV. Additionally, a very low energy loss feature (< 0.5 eV, marked by blue circles in Fig. 4) is found only for the EoD-state spectra of the over-stoichiometric material for incident photon energies 529.0 and 529.5 eV, while it is absent in the corresponding

EoC-state spectra. This feature is also corroborated by the Mn L-RIXS maps for EoD-state spectra discussed below.

C. Mn L-RIXS

In Fig. 5 we display two series of Mn L_3-RIXS maps from the epitaxial thin films with stoichiometric and over-stoichiometric composition, left and right column respectively, during their first lithiation cycle. The incident X-ray energies were chosen around the L_3-absorption peak region above 638 eV at 0.5 eV intervals (Fig. 3). The underlying two-step process is an excitation of a Mn $2p_{3/2}$ core electron into empty $3d$ states, $3d^n$ to $2p^5 3d^{n+1}$, and a subsequent decay of the core hole through different possible channels.

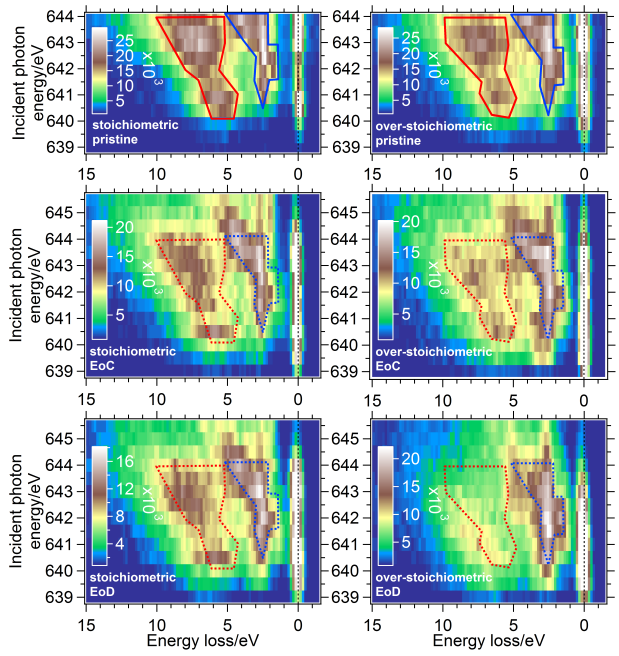

Fig. 5. Left (right) panels show Mn L_3-edge RIXS maps of the stoichiometric (over-stoichiometric) films at different cycle points (top to bottom: pristine, EoC, EoD). The left (bottom) energy scale refers to the incident photon energy (energy loss). To maximize the contrast, the color scale was normalized to begin at the most intense feature in each map (white) and to a common background value for the low point color (blue). The polygons depict areas of interest and are locked to the positions defined in the RIXS maps of pristine films.

In the Mn L_3-RIXS maps of the pristine materials we have marked areas grouped into a low energy loss region (0 to 5 eV, blue polygon) that comprises Mn dd-excitations and a high energy loss region dominated by charge transfer (CT) excitations (>5 eV, red polygon) [18]. In the dd-excitation channel a different $3d$ electron reoccupies the core hole, effectively leaving a reorganized $3d$ band in the final state, $3d^{n*}$. These excitations appear as constant energy loss features regardless of incident photon energy (vertical lines in Fig. 5). CT excitations are the result of ligand electrons refilling the Mn core hole, essentially creating a valence hole $\underline{L}$ on the ligand site and an extra electron in the metal $3d$ band, $3d^{n+1}\underline{L}$. As such, their intensity strongly correlates with the degree of hybridization of the Mn–O bond and, due to the finite size of the O $2p$ band, these excitations exhibit dispersive energy loss features with increasing incident photon energy (diagonal lines in Fig. 5) [19].

Following the lithiation cycle of the over-stoichiometric film material (top to bottom panel of the right column of Fig. 5), we see how the high energy features fade (relative to the most intense feature) when fully delithiated (EoC RIXS map). After subsequent relithiation, the original high energy loss features (red dashed area in EoC RIXS map) are completely gone and instead replaced by other, weaker features e. g. at 7 eV energy loss. In contrast, the stoichiometric film material (panels on left hand side) shows less severe fading when delithiated and remains stable during the entire relithiation. This suggests that profound differences exist between these materials regarding the type of Mn–O bonding that develops during the battery cycling. Clearly, the Mn–O hybridization of the over-stoichiometric film material is weakened during the entire course of the initial cycle. On the other hand, the stoichiometric film material is less prone to changes in Mn–O hybridization strength.

IV. Discussion

The initial delithiation (charging) of the pristine Li_2MnO_3 cathode is known as the *activation phase*. Theoretical studies predict [3] that Li_2MnO_3 is charge-compensated by oxidation of the oxide anion and that localized holes on oxygen (O^-) are formed as the first step that would seem to allow for a reversible anionic redox process. Instead however, transition metal ion migration between the layers, rapid oxygen dimerization, and eventually the formation of molecular oxygen is expected to occur before the next cycle can commence. Experimentally, the detection of oxygen release [20] from the cathode material has corroborated this description.

X-ray absorption spectroscopy by Oishi et al. [4] has revealed the behavior of the O- and Mn-ion states of charge during both the activation and the reversible cycling phase in standard polycrystalline composite material. They concluded that peroxide and superoxide states account for a large part of the reversible charge compensation in Li_2MnO_3, suggesting this also be valid for other layered Li-rich NMC cathode materials. This seems to be a plausible presumption also for our results since both compositions show very similar charge/discharge capacities with a plateau-region at about 4.5 V as well as similar changes of their O K-XAS signatures during cycling. On the other hand, our O K-RIXS analysis shows that there are fundamental differences in the anionic behaviour of Li-rich NMC versus Li_2MnO_3, namely the latter does not show the (reversible) formation of localized holes [2], [21]. Instead, we observe that an irreversible loss of occupied states at the top of the oxygen valence band takes place by the end of the first delithiation. We have analyzed the Mn L-XAS to extract the approximate percentages of different Mn-ion states of charge, i. e. $Mn^{2+}/Mn^{3+}/Mn^{4+}$, and compare to the results of Oishi et al. [4]. The results from

the surface sensitive TEY mode are shown in Fig. 6. We point out that the low fraction of Mn^{2+} that our analysis yields compared to ref. [4] is a result of the normalization process of the reference spectra. We have normalized all XAS-spectra to unit step height whereas Oishi et al. do not specify their normalization procedure, although it appears that the spectra could have been normalized to equal L_3-amplitude height.

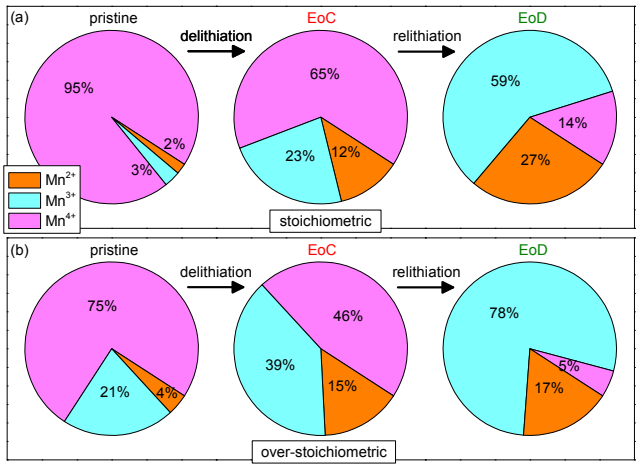

Fig. 6. Mixed oxidation state evolution of Mn ions over the first lithiation cycle of (a) the stoichiometric and (b) the over-stoichiometric Li_2MnO_3 films derived from fits to the surface sensitive TEY spectra. The uncertainty is approximately $\pm 5\%$; best fit simulations along with the underlying reference spectra are shown in Fig. 3.

Our analysis yields that for the pristine stoichiometric film about 95% of the Mn-ions are in a Mn^{4+}-state, which is very close to the formal oxidation state derived assuming purely Li^+- and O^{2-}-ions. Conversely, for the pristine over-stoichiometric film the oxidation state distribution has an unexpectedly high Mn^{3+} contribution compared to the 2%/98% ratio derived from formal sum formula considerations. Delithiation to EoC leaves both films in a mixed distribution where all three oxidation states contribute significantly. We particularly note the substantial increase of the Mn^{2+}-ion fraction. After relithiation to EoD the Mn-ions in the two films are left with dramatically different oxidation state distributions. In both materials we observe an additional, significant increase of the Mn^{3+} as well as some Mn^{2+} contribution, while the 4+ oxidation state contribution shrinks drastically.

Connecting with observations at the O K-edge, we conclude that oxygen bonding properties are very sensitive to the Li/Mn-ratio, resulting in strongly differing O K-XAS spectra after relithiation between both compositions (EoD, Fig. 2). For the stoichiometric film delithiation creates holes that are partially refilled upon relithiation to EoD. In contrast, for the over-stoichiometric film the amount of empty oxygen states close to the Fermi level is significantly smaller after relithiation to EoD than for the pristine material, whereas empty states are created higher above the Fermi level. We note that the character of the peak at 533.8 eV is unclear and could pose an interesting subject for further investigation.

Finally, the Mn L_3-RIXS maps (Fig. 5) show that covalency of the Mn-ions in the over-stoichiometric film weakens significantly, especially upon relithiation. The stark difference between the materials' behaviors in the CT-region during the first cycle also correlates with the long term fading behaviors [7] of the film cathodes. The rapid decline in hybridization seems to foreshadow a capacity fading whereas stable hybridization indicates a favorable pre-condition for a stable cathode capacity.

In summary, we observe that both manganese and oxygen ions participate in the activation process of Li_2MnO_3 as a cathode material. However, the detailed mechanisms depend strongly on their Li/Mn-ratio. While the O K-XAS shows that the stoichiometric material undergoes moderate changes in the conduction band, the over-stoichiometric material shows a more pronounced change of occupancy between de- and relithiated states. On cursory inspection, Mn L-XAS seems to show similar behavior for the films but more detailed fitting analysis shows that, depending on the Li/Mn-ratio, different paths are followed during cycling. Importantly, we find by using Mn L_3-RIXS that the over-stoichiometric cathode material is prone to a rapid loss of Mn–O hybridization whereas the hybridization is significantly more stable in the stoichiometric material. This is concomitant with a restructuring of the O-bonding at the top of the valence band (revealed by O K-RIXS) at the initial delithiation of both materials. While this leaves the stoichiometric material passive upon relithiation, the over-stoichiometric material shows further restructuring at the top of the oxygen band. O K-XAS reveals that holes are formed in the conduction band of both materials. However, in contrast to the localized species that forms in the iso-structural NMC-materials, the created holes in the oxygen band of Li_2MnO_3, regardless of Li/Mn-ratio, have delocalized character.

V. Conclusions

As the first investigation of this kind, we studied the initial cycle behavior of epitaxially grown thin films of Li_2MnO_3 cathode materials using XAS and RIXS. In order to shed more light onto the intricate activation processes of Li_2MnO_3 during its initial lithiation cycle, we studied well-defined crystalline materials without binder and carbon materials of cathodes with two different Li/Mn-ratios of Li_2MnO_3, respectively. Regardless of Li/Mn-ratio, signatures of localized oxygen holes were not observed in O K-RIXS. Instead, the top of the oxygen valence band is depleted of electrons forming delocalized empty states. Another central observation is a rapid loss of Mn–O hybridization in the over-stoichiometric cathode material whereas this hybridization is significantly stabler in the stoichiometric material. These behaviors may serve as indicators for the severity of capacity fading observed in the long term cycling of these cathodes.

More generally, this study shows that RIXS is a powerful technique for retrieving important site-specific information about the cycling behavior of transition metal oxide based battery electrodes. Particularly, studies on epitaxially grown thin film materials constitute an invaluable complementary

source of information about initialization processes and redox reactions by eliminating effects from binder and other additives as well as reducing the surface-to-bulk ratio, encouraging future investigations of other epitaxially grown thin film materials.

ACKKNOWLEDGMENT

REFERENCES

[1] G. Assat and J.-M. Tarascon. "Fundamental understanding and practical challenges of anionic redox activity in Li-ion batteries". In: *Nat. Energy* 3 (2018), pp. 373–386.

[2] K. Luo, M. R. Roberts, R. Hao, et al. "Charge-compensation in $3d$-transition-metal-oxide intercalation cathodes through the generation of localized electron holes on oxygen". In: *Nat. Chem.* 8 (2016), pp. 684–691.

[3] H. Chen and M. S. Islam. "Lithium Extraction Mechanism in Li-Rich Li_2MnO_3 Involving Oxygen Hole Formation and Dimerization". In: *Chem. Mater.* 28.18 (2016), pp. 6656–6663.

[4] M. Oishi, K. Yamanaka, I. Watanabe, et al. "Direct observation of reversible oxygen anion redox reaction in Li-rich manganese oxide, Li_2MnO_3, studied by soft X-ray absorption spectroscopy". In: *J. Mat. Chem. A* 4 (23 2016), pp. 9293–9302.

[5] S. Taminato, M. Hirayama, K. Suzuki, et al. "Highly reversible capacity at the surface of a lithium-rich manganese oxide: a model study using an epitaxial film system". In: *Chem. Commun.* 51 (9 2015), pp. 1673–1676.

[6] K. Hikima, K. Suzuki, S. Taminato, et al. "Thin Film All-solid-state Battery Using Li_2MnO_3 Epitaxial Film Electrode". In: *Chem. Lett.* 48.3 (2019), pp. 192–195.

[7] K. Hikima, S. Taminato, K. Shimizu, et al. "Reaction Mechanism of Li_2MnO_3 for High-Capacity Cathode of Lithium Battery". In: *XXX* xxx (2019). In manuscript.

[8] K. Suzuki, K. Kim, S. Taminato, et al. "Fabrication and electrochemical properties of $LiMn_2O_4$/$SrRuO_3$ multi-layer epitaxial thin film electrodes". In: *J. Power Sources* 226 (2013), pp. 340–345.

[9] R. Qiao, Q. Li, Z. Zhuo, et al. "High-efficiency in situ resonant inelastic x-ray scattering (iRIXS) endstation at the Advanced Light Source". In: *Rev. Sci. Instrum.* 88.033106 (3 2017), pp. 3350–3355.

[10] F. M. F. de Groot, M. Grioni, J. C. Fuggle, et al. "Oxygen $1s$ x-ray-absorption edges of transition-metal oxides". In: *Phys. Rev. B* 40.8 (1989), pp. 5715–5723.

[11] F. M. F. de Groot, M. Abbate, J. van Elp, et al. "Oxygen 1s and cobalt 2p X-ray absorption of cobalt oxides". In: *J. Phys. Condens. Matter* 5 (1993), pp. 2277–2288.

[12] R. Qiao, T. Chin, S. J. Harris, et al. "Spectroscopic fingerprints of valence and spin states in manganese oxides and fluorides". In: *Curr. Appl. Phys.* 13.3 (2013), pp. 544–548.

[13] R. Qiao, K. Dai, J. Mao, et al. "Revealing and suppressing surface Mn(II) formation of $Na_{0.44}MnO_2$ electrodes for Na-ion batteries". In: *Nano Energy* 16.3 (2015), pp. 186–195.

[14] J.-H. Cheng, C.-J. Pan, J.-F. Lee, et al. "Simultaneous Reduction of Co^{3+} and Mn^{4+} in P2-$Na_{2/3}Co_{2/3}Mn_{1/3}O_2$ As Evidenced by X-ray Absorption Spectroscopy during Electrochemical Sodium Intercalation". In: *Chem. Mater.* 26 (2 2014), pp. 1219–1225.

[15] L. A. J. Garvie and A. J. Craven. "High-resolution Parallel Electron Energy-loss Spectroscopy of Mn $L_{2,3}$-Edges in Inorganic Manganese Compounds". In: *Phys. Chem. Minerals* 21 (4 1994), pp. 191–206.

[16] R. Qiao, Y. Wang, P. Olalde-Velasco, et al. "Direct evidence of gradient Mn(II) evolution at charged states in $LiNi_{0.5}Mn_{1.5}O_4$ electrodes with capacity fading". In: *J. Power Sources* 273 (2015), pp. 1120–1126.

[17] L.-C. Duda, J. Downes, C. McGuinness, et al. "Bandlike and excitonic states of oxygen in $CuGeO_3$: Observation using polarized resonant soft-x-ray emission spectroscopy". In: *Phys. Rev. B* 61 (6 2000), pp. 4186–4189.

[18] L. J. P. Ament, M. van Veenendaal, T. P. Devereaux, et al. "Resonant inelastic x-ray scattering studies of elementary excitations". In: *Rev. Mod. Phys.* 83 (2 2011), pp. 705–767.

[19] M. Matsubara, T. Uozumi, A. Kotani, et al. "Charge Transfer Excitation in Resonant X-ray Emission Spectroscopy of NiO". In: *J. Phys. Soc. Jpn.* 74.7 (2005), pp. 2052–2060.

[20] Z. Lu and J. R. Dahn. "Understanding the Anomalous Capacity of Li/Li[$Ni_xLi_{(1/3-2x/3)}Mn_{(2/3-x/3)}$]$O_2$ Cells Using *In Situ* X-Ray Diffraction and Electrochemical Studies". In: *J. Electrochem. Soc.* 149 (7 2002), A815–A822.

[21] K. Luo, M. R. Roberts, N. Guerrini, et al. "Anion Redox Chemistry in the Cobalt Free 3d Transition Metal Oxide Intercalation Electrode Li[$Li_{0.2}Ni_{0.2}Mn_{0.6}$]O_2". In: *J. Am. Chem. Soc.* 138.35 (2016).